RSC Advances

PAPER

View Article Online
View Journal | View Issue

Cite this: *RSC Adv.*, 2023, **13**, 3364

Application of LTA zeolite-modified electrode for sensitive detection of retinoic acid in tap water†

Yuying Jiang,‡[a] Yifeng E,[a] Pengyan Wei,[a] Jia Wang,[a] Peng Chen,[b] Lei Wang,*[c] Thomas F. Krenzel,[d] Kun Qian*[a] and Xiyuan Tong‡[a]

An electrochemical method based on a Linde Type-A zeolite-modified glass carbon electrode (LTA/GCE) was introduced for the determination of retinoic acid (RA). LTA zeolite could be synthesized through a hydrothermal method and served as a commercial electrochemical sensor with high stability and sensitivity in electrochemical progress. The as-synthesized product was characterized by scanning electron microscopy (SEM), differential thermal analysis (DTA), X-ray powder diffraction (XRD), and X-ray photoelectron spectroscopy (XPS). Under optimal conditions, a detection limit of 0.8 μM was obtained for RA with a linear range of 0.8–20.1 μM. This electrochemical method for determining RA was simpler and cheaper than previously reported methods. Furthermore, the modified electrode could be applied to the detection of RA in tap water, achieving a linear range of 1.4–15.0 μM with a detection limit of 1.4 μM and good recovery. The modified electrode designed by this method provided good selectivity, stability, and reproducibility for RA determination and reliable application for the analysis of RA in environmental water.

Received 23rd September 2022
Accepted 19th December 2022

DOI: 10.1039/d2ra06011f

rsc.li/rsc-advances

Introduction

Retinoic acid (RA) is considered to be one of the primary active metabolites of vitamin A that regulates various biological processes. It is widely used for the local treatment of various skin diseases, such as acne[1] and psoriasis.[2] RA made significant progress in differentiation treatment, which has made it the preferred drug for the treatment of acute promyelocytic leukemia (APL).[3] As a result of its differentiation, anti-proliferation, and pro-apoptosis,[4] RA and its derivatives have been widely used for other cancers such as hepatoma, lung cancer, and breast cancer.[5–7] A lower level of RA may cause cell cycle stagnation.[5] Additionally, the application of RA is limited by the chemical properties of photodegradation, oxidation, and thermal sensitivity, which is one of the reasons why the detection of RA has always been a hard nut to crack in scientific research.

Continuous efforts have been put into the detection of RA. Nearly all advanced methods have been applied to achieve a better result, including the high-performance liquid chromatographic method (HPLC),[8–11] spectrophotometric method,[12–15] and liquid chromatography-mass spectrometry (LC-MS).[16–18] These methods have made noticeable advances in sensitivity and specificity. The electrochemical method was introduced for the detection of RA by deposited metal electrodes in 2000.[19] The modified electrode further improved detection in an actual sample with more specificity through the DPV (differential pulse voltammetry) method.[20] Additionally, breakthrough progress was achieved for human urine and plasma samples in 2020 by the ASV (anodic stripping voltammetry) method.[21] As far as we know, only the last three research papers were reported in the last decade within the electrochemistry method domain for RA detection (Table S1†). In this field, it is still a challenge to produce novel electrode materials and suitable electrochemical methods to improve sensitivity, accuracy, simple operation without pretreatment, low cost, and a fast response time in real-time analysis.[22]

With the development of electrochemical sensors, an increasing number of functional materials are being used to detect vitamins and their derivatives. These include materials such as carbon nanotubes (CNTs), graphene, reduced graphene oxide (rGO), and metal nanoparticles.[23–26] However, the application of the aforementioned nanomaterials in electrode modification may be limited by some of their drawbacks, such as the instability of metal oxide nanoparticles, their biological toxicity, explosiveness, and negative impact on the environment.

[a]*College of Pharmacy, Jinzhou Medical University, Jinzhou, Liaoning, P. R. China. E-mail: skyearth20032003@163.com*

[b]*Key Laboratory of Functional Inorganic Material Chemistry, School of Chemistry and Materials Science, Heilongjiang University, Harbin, Heilongjiang, P. R. China*

[c]*Changchun Institute of Applied Chemistry, Chinese Academy of Science, Changchun 130022, P. R. China*

[d]*Materials Engineering, Faculty Technology and Bionics, Rhine-Waal University of Applied Sciences, Kleve D-47533, Germany*

† Electronic supplementary information (ESI) available. See DOI: https://doi.org/10.1039/d2ra06011f

‡ Dr Xiyuan Tong contributes equally with Yuying Jiang in this work.

Similarly, carbon-based materials have some limitations in sensor fabrication due to their structural features and properties such as chemical activation, surface functionalization, defects, and particle aggregation. Zeolites have a specific framework structure with a wide range of micro- and mesoporous, natural, or synthetic crystalline hydrated aluminum silicates. Zeolites have unique molecular sieving properties as well as high cation exchange capacity (CEC), which have been utilized in the development of novel electrochemical sensors for different organic, inorganic and pharmaceutical compounds.

Compared with reported electrodes, zeolite material is a good candidate with higher stability and lower cost. Zeolite is an advanced material that is widely used in the petrol industry for its adjustable acid catalyst sites, stable framework structure, high adsorption capability, and nano-sized pore window.[27–29] Linde Type-A (LTA) zeolite is a stable framework structure with an open-pore window scale in the range of 0.4 to 0.6 nanometers.[30] The SiO_4 and AlO_4 tetrahedra are connected by oxygen atoms.[31] Due to its unique pore and cage structure, LTA zeolite is used to adsorb guest molecules of specific sizes and shapes.[32] In this work, the RA molecules were adsorbed on the electrode surface using LTA zeolite. The DPV method was used to detect the concentration of RA in phosphate buffer solution (PBS) and tap water with sensitivities of 0.8 and 1.4 μM, and linear ranges of 0.8–20.1 μM and 1.4–15.0 μM. The highly crystalline material showed high stability in both thermal and electrochemical conditions. As the LTA zeolite material has been widely used in industrial production, the zeolite-modified electrode may promise favorable commercial prospects.

Experimental

Instruments

A TDM-10 powder X-ray diffractometer (XRD) (Dandong Tongda, China) with 40 kV 30 mA Cu Kα radiation was used to identify the as-synthesized product and the samples calcined at different temperatures. The SEM pictures were taken with a Hitachi S4800 scanning electron microscope (SEM) (Hitachi Limited, Japan). The differential thermal analysis (DTA) curve was obtained by using HCR-4 microcomputer differential calorimeter (Beijing Hengjiu, China) to record the endothermic and exothermic peaks obtained at a heating rate of 10 K per minute. LTA zeolite samples at different temperatures were calcined using a KSW resistor furnace temperature controller (Hebei Chengde, China). X-ray photoelectron spectroscopy (XPS) (KRATOS, England) analysis was performed on an AXIS Ultra^{DLD} analyzer. Electrochemical characterization was carried out on the CHI 650 measurement (Shanghai Chenhua). A glass carbon electrode (GCE) covered by a layer of LTA zeolite was selected as the working electrode. The counter electrode was a Pt wire electrode. The reference electrode was a saturated calomel electrode (SCE).

Chemicals

The chemicals used were: RA (98%, Shanghai Aladdin Biochemical Technology Co., Ltd); sodium aluminate ($NaAlO_2$, Liaoning Quanrui Reagent Co., Ltd); sodium hydroxide (NaOH, Tianjin Tianli Chemical Reagent Co., Ltd); sodium silicate (Na_2SiO_3, Wuxi Yatai United Chemical Industry); potassium hexacyanoferrate ($K_3Fe(CN)_6$, Tianjin Damao Chemical Reagent Co., Ltd); and potassium chloride (KCl, Tianjin Yongsheng Fine Chemical Industry Co., Ltd). All the chemicals were used as received. Tap water was obtained from a laboratory tap without further purification.

Methods

The synthesis of LTA zeolite. The synthesis of LTA zeolite adopted an improved literature method.[33] The LTA zeolite was prepared as follows: 0.75 g of NaOH, 0.70 g of Na_2SiO_3, and 0.60 g of $NaAlO_2$ were mixed with 18 mL of distilled water under continuous stirring. After the system was evenly mixed, the gel was transferred into a Teflon reactor with steel and crystallized at 373 K for 24 hours with stirring. The gel was washed with distilled water and ethanol. The obtained solid sample was dried at room temperature overnight to obtain the white crystal.

Preparation of modified electrodes. The working electrode was prepared as follows: the bare GCE electrode was polished with 0.3 and 0.05 mm alumina slurry, ultrasonically washed with water and ethanol, and blow dried with high-purity nitrogen at room temperature. Subsequently, 20 mg of LTA zeolite crystal was dispersed into 0.5 mL of ethanol with the help of ultrasound for half an hour. Then 20 μL of the suspension was dropped onto this mirror-like GCE electrode, and the ethanol was evaporated by blowing N_2 at room temperature. All the following experiments were performed in PBS solution at 298 K under N_2 protection. The DPV method was performed to collect information about the related potential and current data in different concentrations of RA. Cyclic voltammetry (CV) was carried out to distinguish the mechanism of the electrochemical progress from adsorption to diffusion. The amperometric *i–t* curve (A *i–t* C) was applied to test the electrochemical stability of the LTA/GCE electrode.

Electrochemical measurements. Sodium dihydrogen phosphate (NaH_2PO_4) and dibasic sodium phosphate ($Na_2HPO_4 \cdot 3H_2O$) were prepared to obtain the 0.1 M phosphate buffer solutions (PBS), and the whole experiment was performed in pH 8 PBS solution at 298 K under N_2 protection. During each test, 5 mL of electrolyte was placed in the electrolytic cell, in which the working electrode, counter electrode, and reference electrode were introduced. Cyclic voltammetry (CV) was selected to study

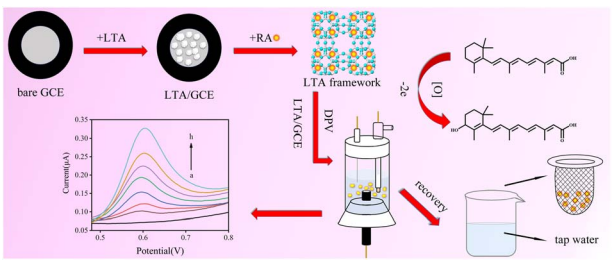

Scheme 1 The reaction mechanism of the detection of RA.

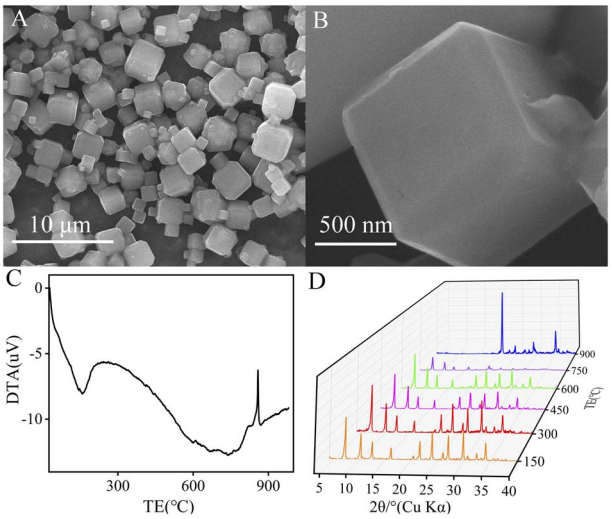

Fig. 1 (A) The SEM picture of LTA zeolite with a larger scale. (B) The SEM picture of LTA zeolite for a single crystal. (C) The DTA curve of the LTA zeolite for the temperature from 25 to 1000 °C. (D) The XRD patterns of the LTA zeolite calcined for 6 hours at 150, 300, 450, 600, 750 and 900 °C, respectively.

the electrochemical process of RA in the potential range of 0.4–1.0 V at the scan rate of 100 mV s^{-1}, then distinguished the mechanism of the electrochemical progress from adsorption to diffusion by changing the scan rate (50–200 mV s^{-1}) and the pH value of PBS (5.7–8.0). The DPV method was performed to collect information about the related potential and current data in RA of different concentrations (0.8–20.1 μM) in the potential range of 0.4–1.0 V, and the amplitude was 0.05 V. The Amperometric *i–t* Curve (A *i–t* C) was applied to test the electrochemical stability of the LTA/GCE electrode, and the initial *E* was −1.0 V.

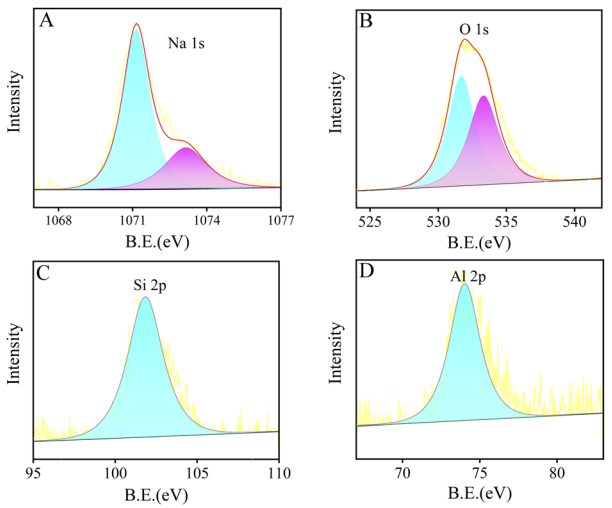

Fig. 2 The XPS spectra of Na 1s, O 1s, Si 2p, Al 2p in LTA zeolite are shown in (A), (B), (C), and (D), respectively.

Results and discussion

The characterization of LTA zeolite

The LTA zeolite is synthesized in hydrothermal conditions and coated on the surface of the GCE electrode to serve as a detection electrode (Scheme 1). The LTA zeolite is a kind of aluminosilicate material with a specific skeleton structure and a large number of micropores and mesopores. Their unique molecular sieve characteristics provide shape and size differentiation. Their open channel windows allow ion exchange of electrically active substances, thus providing adsorption and desorption capabilities, and are usually used to adsorb organic and non-organic toxic substances. In recent years, this catalytic reaction characteristic has led to the wide application of zeolite materials in electrochemical sensors. Its adsorption capacity is also appropriate in electrochemical processes. Previously, it was reported that zeolite could be used as an effective adsorbent for vitamins.[3] RA molecules contained easily ionized carboxylic acid groups, which could be selectively adsorbed on the LTA/GCE electrode. When detected by the DPV method, a large amount of RA enrichment on its surface could significantly

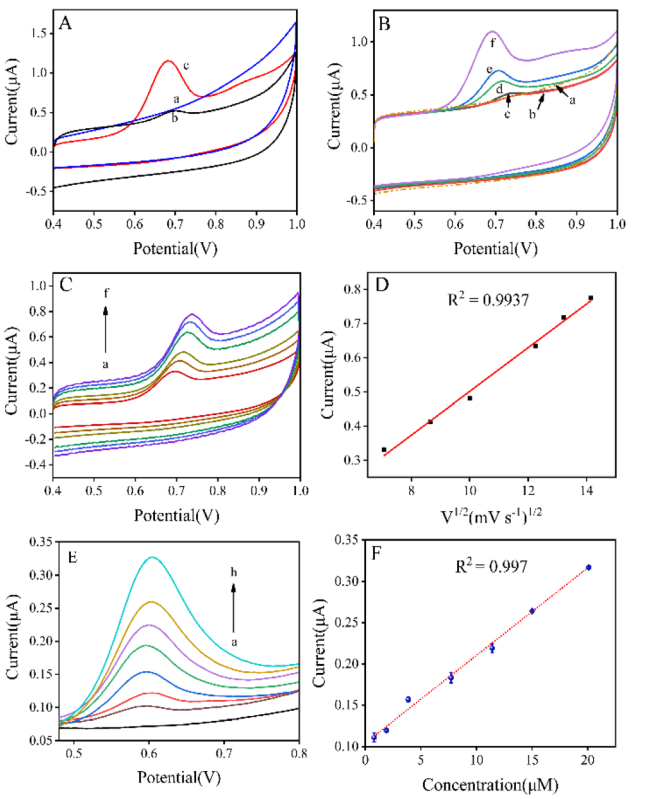

Fig. 3 (A) CVs of LTA zeolite without RA (a), bare GCE electrode (b) and LTA/GCE electrode (c) containing 20 μM RA in 0.1 M PBS (pH 8.0) at a scan rate of 100 mV s^{-1}. (B) CV curves (curve a–f) of LTA/GCE electrode in 0.1 M PBS containing 20 μM RA with different pH values (5.7 to 8). (C) CV curves of LTA/GCE at the scan rate of 50–200 mV s^{-1}. (D) The linear relationship between current peaks and the square roots of scan rates. (E) DPV response obtained for the LTA/GCE electrode upon the addition of RA of different concentrations. (F) The linear relationship between peak current and the concentration of RA.

enhanced the electrochemical signal of its oxidation process. At this time, the voltammetric peak obtained from the electrochemical oxidation process of RA may be the hydroxylation at position C-4 of the cyclohexenyl moiety to form the 4-hydroxyl-RA.[34,35] On this basis, the sensor was successfully used to detect RA in tap water, and RA in tap water by the standard method was assessed for a good recovery.

The morphologies of the LTA zeolite were characterized by SEM. As seen from the SEM images (Fig. 1A and B), the main morphology of the LTA zeolite is cubic. The crystal size is unique in the main range of *ca.* 1–5 micrometers. The polycrystalline diffraction data are collected on the XRD detector to identify the phase of the product, as shown in Fig. S1.† By comparing the peak position of the patterns between the as-synthesized LTA and the simulated one, it is found that they are a good match, suggesting phase purity.

The DTA thermogram is used to evaluate the stability of the sample, and the result is shown in Fig. 1C. The peak at *ca.* 150 °C indicates that the absorbed water has been released from the nanosized pore of LTA upon heating. Additionally, the sharp peak at 858 °C corresponds to the collapse of the framework, which is confirmed by Fig. 1D at 900 °C. By comparing the XRD patterns after calcination at different temperatures, the result shows that the peaks at 300 °C are higher than those calcined at other temperatures. The results shows that the sample calcined at 300 °C has the best crystallinity. Crystal formation is lowest for samples calcined at 750 °C. At 900 °C, it is difficult to observe the diffraction peaks before 20°. The results illustrate that the structure has been destroyed. The LTA zeolite calcined at different temperatures is used to modify the GCE electrode. The DPV diagrams of 10 μM RA in Fig. S2† show that the uncalcined LTA zeolite reaches a maximum current value of 2.4 μA. While other LTA zeolites calcine at different temperatures obtain relatively lower currents. The results illustrate that the modified electrode can maintain high electrochemical activity and stable operation at high temperatures even after calcination.

To investigate the properties of the various elements in the LTA zeolite, the material is further studied using XPS, and the collected data is shown in Fig. 2. The binding energy (B.E.) of the Na element of the LTA zeolite is shown in Fig. 2A, exhibiting the characteristic peaks indexed to the 1s orbital. The two peaks of the O element demonstrate the different coordination states of the oxygen atoms within the LTA framework and water molecules sited in the channel (Fig. 2B). The XPS spectra of the framework elements Si and Al are given in Fig. 2C and D. Both Si and Al peaks can be indexed to the 2p orbitals, which confirms that the sample of LTA is of pure phase and the tetrahedral Si/Al atoms are in their stable four-fold coordination state.

The electrochemical activity of RA in the CV method

The electrode activity of RA on the GCE electrode and LTA/GCE electrode was tested by the CV method in PBS. As shown in Fig. 3A, curve a represents a smooth background curve without peaks given by the LTA/GCE electrode in PBS 8 without RA. Cyclic voltammograms (CVs) of 20 μM RA in the buffer solution is obtained with the GCE electrode (curve b) and LTA/GCE

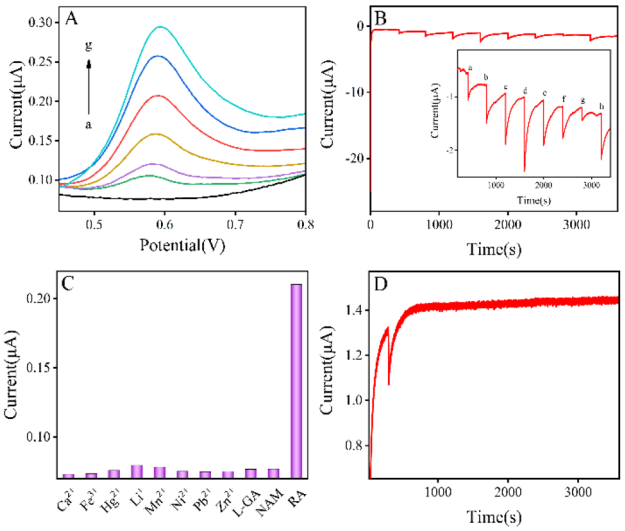

Fig. 4 (A) DPV response obtained for the LTA/GCE electrode upon the addition of RA of different concentrations in 5 mL of PBS (pH 8.0) and 5 mL of tap water. (B) A *i*–*t* C obtained for the addition of 2 μM RA; (C) the effect of common interfering ions and molecules presented in PBS solutions at pH 8 for the determination of RA. (D) A *i*–*t* C of the 20 μM RA being reduced at 3600 s on the LTA/GCE electrode with the initial potential of −1.0 V.

electrode (curve c); the current peak of LTA zeolite can be observed at 0.68 V while that of the GCE electrode was at 0.70 V. The GCE electrode as a substrate exhibits relatively low background currents for RA oxidation. When the surface of the GCE electrode is covered by the LTA zeolite layer, a clear signal for RA oxidation peak analysis is observed. The RA is oxidized on the electrode surface to form a 4-hydroxyl-RA. The result of the current peaks reveals that the LTA/GCE electrode is more active than the bare GCE electrode for the determination of RA. The CV curve is recorded in 0.1 M PBS (pH 8.0) containing 20 μM RA, and only the anodic peak of oxidation of RA is observed. The absence of a cathodic peak indicates that the process was chemically irreversible.

Effect of pH value and scan rate

The effect of the pH of PBS on the current signal is shown in Fig. 3B. During the oxidation of RA, the separation of electrons and protons leads to the formation of its oxidation products. As the pH value increases, the peak potential moves toward more negative values. It indicates that protons have been involved in the oxidation process of RA. In addition, the functional groups present in the RA molecule may be involved in acid–base and hydration equilibria. Therefore, the choice of pH of PBS is also a relatively important condition. Keeping the pH of PBS between 5.7 and 8.0, the peak current depends on the pH of the buffer solution. When the pH value of the PBS solution shifts from 5.7 to 8 (curve a–e), the related peak current shifts from 0.5 to 1.1 μA. Therefore, 0.1 M PBS (pH 8.0) is chosen as the best supporting electrolyte and has been used for further measurements. The current peak value of oxidation curves is enlarged as the scan rate is accelerated from 50 to 200 mV s^{-1} while the RA

Table 1 The RSD of the detection for RA in tap water

Added concentration (μM)	Detected concentration (μM)	Detected current (μA)	Recovery (%)	RSD (%) $n = 4$
7.7	7.82	0.207	101.6	6.45
	7.76	0.206	100.7	
	7.69	0.205	99.8	
	6.79	0.192	88.2	
11.4	11.28	0.258	99.0	3.65
	10.67	0.249	93.6	
	11.35	0.259	88.6	
	10.58	0.248	92.8	

concentration is 20 μM (Fig. 3C). The linear regression equation is simulated by the square root of scan rates and the current peaks in Fig. 3D. The peak current of the RA oxidation process increases linearly with the scan rate. The CVs and the linear regression equation reveal the diffusion control process, as the current is proportional to the square root of the scan rate with an R^2 of 0.9937. The results indicate that the oxidation of RA is controlled by adsorption at a pH value of 8. Adsorption control results in an expected slope of 2.872, which denotes that RA is adsorbed on the surface of the LTA/GCE electrode.

Electrochemical detection of RA on LTA/GCE electrode

The voltammetric response of the LTA/GCE electrode at different concentrations of RA is investigated by the DPV method (shown in Fig. 3E). Curve a shows the background with the LTA/GCE electrode in PBS; then the current peak is raised from 0.1 to 0.3 μA (curves b–h). The intensity of the current increases significantly with RA concentration. The relationship between the current peaks and the RA concentration is simulated with a linear regression equation (Fig. 3F): the slope is 0.011 with an R^2 of 0.997. The linear regression equation indicates the potential for the determination of RA at concentrations of 0.8–20.1 μM. Compared to the previously reported electrode sensing performance (Table S1†), a wider linear range is obtained for the LTA/GCE sensor. The LTA/GCE electrode is highly sensitive to RA detection using the DPV method. In the electrochemical detection of RA, there are many interfering factors from the sample, buffer, electrode, circuit, *etc.* Therefore, electrode materials with high physicochemical stability as well as high sensitivity and selectivity to the target vitamins should be selected. At the same time, the prepared electrodes should have high consistency and structural stability. It is worth noting that the surface area of the electrode, has a great influence on the electrochemical response of the sensor. LTA zeolite can provide a high active surface area to enhance the contact between the electrode and the working electrolyte, and also promote more active sites to participate in the electrochemical reaction, which has good application prospects.

Electrochemical detection of RA in tap water

To investigate and analyze the potential application of LTA zeolite modified electrodes, the concentration of RA was determined by the DPV method using tap water as a real sample. First, 5 mL of tap water was added to PBS (5 mL) with various concentrations of RA on the LTA/GCE electrode. In Fig. 4A, curve a represents the background. The anodic peak current increases with increasing the RA concentration in the solution (curve b–g). In the concentration range of 1.4 to 15.0 μM, the current peak rises from 0.1 to 0.3 μA while the potential shifts from 0.58 to 0.59 V. The linear regression equation between peak current and RA concentration is shown in Fig. S3A.† The slope is 0.015 with an R^2 of 0.995. The result is similar to that in PBS (pH 8.0), proving its reproducibility in tap water.

The specific detection performance of the LTA/GCE electrode

The amperometric *i–t* curve (A *i–t* C) method was used to further test the LTA/GCE electrode for 3600 s with an initial potential of −1.0 V. The method was also performed to test LTA/GCE electrode sensitivity for the determination of RA in PBS solution at pH 8. At the first 400 s, the reaction time is used to stabilize the LTA electrode without the addition of RA as the baseline. After that, 10 μM of RA solution (100 μL) is added to the reaction system, and the final current value is recorded again for another 400 s of A *i–t* C method running time, as shown in Fig. 4B (see the inset). The concentration of RA solution is in the range of 0 to 12.3 μM while the final stable current reduces from −0.6 to −1.4 μA in Fig. S3B.† After the final 400 s, the current drops in a step shape (Fig. 4B). The above results show that the LTA/GCE electrode reveals good stability for the determination of RA, and can serve as a potential electrochemical sensor.

Selectivity of the LTA/GCE electrode to the external environment and various interferences is essential for practical analysis. A series of interference experiments were carried out to investigate the current response of these compounds for RA at a potential of 0.6 V. The concentration of interfering substances was set at 10 μM for Ca^{2+}, Fe^{3+}, Hg^{2+}, Li^{+}, Mn^{2+}, Ni^{2+}, Pb^{2+}, Zn^{2+}, L-glutamate (L-GA), and nicotinamide (NAM). The experiments are also performed on the LTA/GCE electrode under the same reaction condition as for RA (Fig. 4C). Due to the current peak of RA being *ca.* 20 times higher than those of other ions and molecules, the detection sensitivity of the modified electrode is higher than those of the interfering substances which have been tested. The results indicate that the LTA/GCE electrode reveals good selectivity, which allows for the detection of RA in real samples.

The A *i–t* C method is used to test the stability of the LTA/GCE electrode, and the reduction time is set to 3600 s at an initial potential of −1.0 V (Fig. 4D). The graph shows that the current fluctuates after 300 s when 10 μM RA is added, which denotes that the modified electrode kept running smoothly. The results illustrate that the LTA/GCE electrode can be kept stable in the electrochemical process.

The stability of the LTA/GCE electrode was re-determined by the CV method. The CVs of the LTA/GCE electrode in 1 mM $K_3Fe(CN)_6$ and 0.1 M KCl solution cyclically scan for 100 segments are shown in Fig. S4.† The CV curve fluctuates greatly in the first segment, and then basically remains stable. This result indicates that the LTA zeolite tends towards stability at the end.

An error chart is drawn based on the relationship between the concentration of RA and the current peaks in the DPV method, as shown in Fig. 3E. The intensity of the current increases significantly with the RA concentration. The linearity is set by the DPV method in a range of 0.8 to 20.1 μM. The precision of this method is evaluated in tap water with a range of 1.4 to 15.0 μM for RA. At this level, the relative standard deviations (RSDs) are calculated and are listed in Table 1. As it is difficult to find samples with suitable concentration ranges in nature, the standard addition method is chosen to detect drugs in tap water with 7.7 and 11.4 μM of RA to verify the feasibility of the scheme. The results show that the calculated values are extremely close to those expected. The recovery obtained goes from 88.2% to 101.6% with an RSD of 6.45% for the concentration 7.7 μM ($n = 4$), while it goes from 88.6% to 99.0% with an RSD of 3.65% for a concentration of 11.4 μM ($n = 4$). Therefore, the proposed method is suitable for the detection of RA.

Conclusions

The LTA zeolite was synthesized in hydrothermal conditions to produce highly crystalline microporous materials and served as a modified working electrode for the voltammetric detection of RA. It was found that the LTA/GCE electrode exhibited good sensitivity and could be used for the analysis of RA in tap water. It also revealed reasonable selectivity for various kinds of interfering substances with good reproducibility and stability. As the LTA/GCE electrode reaction route was low cost and convenient for commercial production, the study may provide some ideas for the development of novel electrochemical sensors for RA detection.

Author contributions

Yuying Jiang: writing-original draft preparation. Xiyuan Tong: reply to editor and reviewer. Yifeng E and Kun Qian: conceptualization, methodology, writing-review, funding acquisition. Pengyan Wei and Jia Wang: validation, formal analysis. Peng Chen: writing-review, characterization of SEM and XPS for LTA zeolite. Lei Wang: investigation and software. Thomas F. Krenzel: editing.

Conflicts of interest

There are no conflicts to declare.

Acknowledgements

This work is supported by the National Natural Science Foundation of China (Grant No. 21701069), the China Scholarship Council (Grant No. 20160821004), Natural Science Foundation of Liaoning Province (Grant No. 2022020314-JH2/1013), the Department of Education of Liaoning Province (Grant No. JYTJCZR2020082), and Liaoning Provincial Key Laboratory of Marine Bioactive Substances and Technological Innovation Center of Liaoning Pharmaceutical Action and Quality Evaluation (Grant No. 2022–06).

References

1 S. Veraldi, M. Barbareschi, S. Benardon and R. Schianchi, *J. Dermatol. Treat.*, 2013, **24**, 374–376.
2 W. Wang, G.-f. Shu, K.-j. Lu, X.-l. Xu, M.-c. Sun, J. Qi, Q.-l. Huang, W.-q. Tan and Y.-z. Du, *J. Nanobiotechnol.*, 2020, **18**, 1–14.
3 Siddikuzzaman, C. Guruvayoorappan and V. Berlin Grace, *Immunopharmacol. Immunotoxicol.*, 2011, **33**, 241–249.
4 T. Schenk, S. Stengel and A. Zelent, *Br. J. Cancer*, 2014, **111**, 2039–2045.
5 M.-C. Chen, S.-L. Hsu, H. Lin and T.-Y. Yang, *Biomedicine*, 2014, **4**, 1–6.
6 H. Fernandes-Silva, H. Araújo-Silva, J. Correia-Pinto and R. S. Moura, *Biomolecules*, 2020, **10**, 152.
7 S. Alsafadi, C. Even, C. Falet, A. Goubar, F. Commo, V. Scott, V. Quidville, L. Albiges, M.-V. Dieci and J. Guegan, *Clin. Breast Cancer*, 2013, **13**, 401–408.
8 C. M. Teglia, M. D. G. García, M. M. Galera and H. C. Goicoechea, *J. Chromatogr. A*, 2014, **1353**, 40–48.
9 B. M. Tashtoush, E. L. Jacobson and M. K. Jacobson, *J. Pharm. Biomed. Anal.*, 2007, **43**, 859–864.
10 F. Ibrahim, M. K. Sharaf El-Din, A. K. El-Deen and K. Shimizu, *J. Chromatogr. Sci.*, 2019, **57**, 495–501.
11 A. Mahmoudi and M. S. Boukhechem, *Sep. Sci. plus*, 2020, **3**, 86–93.
12 M. Bordbar, A. Yeganeh-Faal, J. Ghasemi, M. Ahari-Mostafavi, N. Sarlak and M. Baharifard, *Chem. Pap.*, 2009, **63**, 336–344.
13 E. S. Elzanfaly, A. S. Saad and A.-E. B. Abd-Elaleem, *Saudi Pharm. J.*, 2012, **20**, 249–253.
14 M. B. Tehrani, M. Namadchian, S. F. Vatan and E. Souri, *Daru, J. Pharm. Sci.*, 2013, **21**, 1–7.
15 M. R. Elghobashy, L. I. Bebawy, R. F. Shokry and S. S. Abbas, *Spectrochim. Acta, Part A*, 2016, **157**, 116–123.
16 J.-B. Peng, C.-H. Luo, Y.-C. Wang, W.-H. Huang, Y. Chen, H.-H. Zhou and Z.-R. Tan, *Molecules*, 2014, **19**, 1189–1200.
17 D. K. Bempong, I. L. Honigberg and N. M. Meltzer, *J. Pharm. Biomed. Anal.*, 1995, **13**, 285–291.
18 X. Wu, J. Hu, A. Jia, H. Peng, S. Wu and Z. Dong, *Environ. Toxicol. Chem.*, 2010, **29**, 2491–2497.

19 L.-H. Wang, *Anal. Chim. Acta*, 2000, **415**, 193–200.
20 F. L. O. da Silva, L. M. da Silva Tinoco, L. A. M. Ferreira, A. R. Malagutti and G. Carneiro, *Anal. Chim. Acta*, 2015, **182**, 929–934.
21 A. F. Alghamdi, *J. King Saud Univ., Sci.*, 2020, **32**, 2635–2640.
22 V. K. Gupta, R. Jain, K. Radhapyari, N. Jadon and S. Agarwal, *Anal. Biochem.*, 2011, **408**, 179.
23 S. Gheibi, H. Karimi-Maleh, M. A. Khalilzadeh and H. Bagheri, *J. Food Sci. Technol.*, 2015, **52**, 276–284.
24 F. Li, J. Li, Y. Feng, L. Yang and Z. Du, *Sens. Actuators, B*, 2011, **157**, 110–114.
25 F. Wu, T. Huang, Y. Hu, X. Yang, Y. Ouyang and Q. Xie, *Microchim. Acta*, 2016, **183**, 2539–2546.
26 D. R. Kumar, D. Manoj, J. Santhanalakshmi and J.-J. Shim, *Electrochim. Acta*, 2015, **176**, 514–522.
27 M. Yabushita, H. Kobayashi, A. Neya, M. Nakaya, S. Maki, M. Matsubara, K. Kanie and A. Muramatsu, *CrystEngComm*, 2020, **22**, 7556–7564.
28 X. Chen, R. Jiang, Y. Gao, Z. Zhou and X. Wang, *CrystEngComm*, 2021, **23**, 2793–2800.
29 D. Yuan, Q. Wang, Y. Shang, H. Liu and A. Xing, *CrystEngComm*, 2021, **23**, 2504–2508.
30 F. Collins, A. Rozhkovskaya, J. G. Outram and G. J. Millar, *Microporous Mesoporous Mater.*, 2020, **291**, 109667.
31 H. V. Doan, K. M. Leung, V. P. Ting and A. Sartbaeva, *CrystEngComm*, 2021, **23**, 857–863.
32 Y. Li, H. Cao and J. Yu, *Acs Nano*, 2018, **12**, 4096–4104.
33 Z. Xue, J. Ma, W. Hao, X. Bai, Y. Kang, J. Liu and R. Li, *J. Mater. Chem.*, 2012, **22**, 2532–2538.
34 N. Y. Kedishvili, *Subcell. Biochem.*, 2016, 127–161.
35 A. C. Ross, *J. Nutr.*, 2003, **133**, 291S–296S.